A Catalytic Diad Involved in Substrate-Assisted Catalysis: NMR Study of Hydrogen Bonding and Dynamics at the Active Site of Phosphatidylinositol-Specific Phospholipase C†

Margret Ryan, Tun Liu,‡ Frederick W. Dahlquist, and O. Hayes Griffith*

Institute of Molecular Biology and Department of Chemistry, University of Oregon, Eugene, Oregon 97403

Received May 10, 2001; Revised Manuscript Received June 15, 2001

ABSTRACT: Phosphatidylinositol-specific phospholipase Cs (PI-PLCs, EC 3.1.4.10) are ubiquitous enzymes that cleave phosphatidylinositol or phosphorylated derivatives, generating second messengers in eukaryotic cells. A catalytic diad at the active site of *Bacillus cereus* PI-PLC composed of aspartate-274 and histidine-32 was postulated from the crystal structure to form a catalytic triad with the 2-OH group of the substrate [Heinz, D. W., et al. (1995) *EMBO J. 14*, 3855−3863]. This catalytic diad has been observed directly by proton NMR. The single low-field line in the ^{1}H NMR spectrum is assigned by site-directed mutagenesis: The peak is present in the wild type but absent in the mutants H32A and D274A, and arises from the histidine $H^{\delta 1}$ forming the Asp274−His32 hydrogen bond. This hydrogen is solvent-accessible, and exchanges slowly with H_2O on the NMR time scale. The position of the low-field peak shifts from 16.3 to 13.8 ppm as the pH is varied from 4 to 9, reflecting a pK_a of 8.0 at 6 °C, which is identified with the pK_a of His32. The $H^{\delta 1}$ signal is modulated by rapid exchange of the $H^{\epsilon 2}$ with the solvent. Estimates of the exchange rate as a function of pH and protection factors are derived from a line shape analysis. The NMR behavior is remarkably similar to that of the serine proteases. The postulated function of the Asp274-His32 diad is to hydrogen-bond with the 2-OH of phosphatidylinositol (PI) substrate to form a catalytic triad analogous to Asp-His-Ser of serine proteases. This is an example of substrate-assisted catalysis where the substrate provides the catalytic nucleophile of the triad. This hydrogen bond becomes shorter as the imidazole is protonated, suggesting it is stronger in the transition state, contributing further to the catalytic efficiency. The hydrogen bond fits the NMR criteria for a short, strong hydrogen bond, i.e., a highly deshielded proton resonance, bond length of 2.64 ± 0.04 Å at pH 6 measured by NMR, a D/H fractionation factor significantly lower than 1.0, and a protection factor ≥100.

Phosphatidylinositol-specific phospholipase C (PI-PLC)[1] plays a central role in signal transduction initiated by binding of many polypeptide hormones, growth factors, and neurotransmitters to their receptors on plasma membranes of eukaryotic cells (*1*). These enzymes cleave phosphorylated forms of the specialized lipid phosphatidylinositol to form second messengers, which mediate the activation of protein kinase C and release of intracellular Ca^{2+} (*2*). PI-PLCs are produced by a variety of aerobic or anaerobic Gram-positive bacteria, including the pathogens *Bacillus cereus*, *B. thuringiensis*, *Listeria monocytogenes*, *L. ivanovii*, *Staphylococcus aureus*, *Clostridium novyi*, and *Rhodococcus equii*. These enzymes are possible virulence factors. Bacterial PI-PLCs catalyze the cleavage of the lipid phosphatidylinositol (PI) into two parts: *myo*-inositol 1,2-cyclic phosphate (cIP) and diacylglycerol (Figure 1). In a second reaction, the enzyme carries out a much slower hydrolysis, opening the ring of cIP to form *myo*-inositol 1-phosphate, I(1)P. In contrast to the eukaryotic isozymes, bacterial PI-PLCs also have the ability to cleave the glycosyl-PI anchor of proteins tethered to eukaryotic cell membranes by glycosylphosphatidylinositol (GPI) anchors. Due to their small size (35 kDa), these enzymes are emerging as an important model system for the

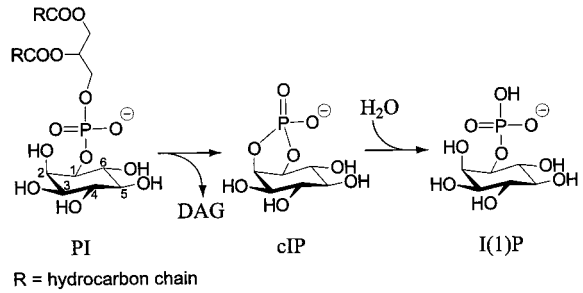

FIGURE 1: The two reactions catalyzed by PI-specific phospholipase C. The first step is a rapid phosphotransferase reaction in which the phospholipid is cleaved into two parts: the lipid-soluble diacylglycerol (DAG) and the water-soluble component (cIP). The second step is a cyclic phosphodiesterase activity, a slow hydrolysis reaction which opens the ring of the cyclic phosphate to form I(1)P. R, hydrocarbon chain.

† This work was supported by NIH Grant GM25698 to O.H.G.

* Corresponding author. E-mail: hayes@molbio.uoregon.edu. Phone: (541) 346-4634. Fax: (541) 346-5891.

‡ Present address: The R. W. Johnson Pharmaceutical Research Institute, P.O. Box 300, Raritan, NJ 08869.

[1] Abbreviations: DSS, 2,2-dimethyl-2-silapentane-5-sulfonate, sodium salt; cIP, D-*myo*-inositol 1,2-cyclic phosphate; kbp, kilo base pair(s); PI, phosphatidylinositol; PI-PLC, phosphatidylinositol-specific phospholipase C; SSHB, short, strong hydrogen bond; Tris, tris(hydroxymethyl)aminomethane.

10.1021/bi010958m CCC: $20.00
Published on Web 07/18/2001

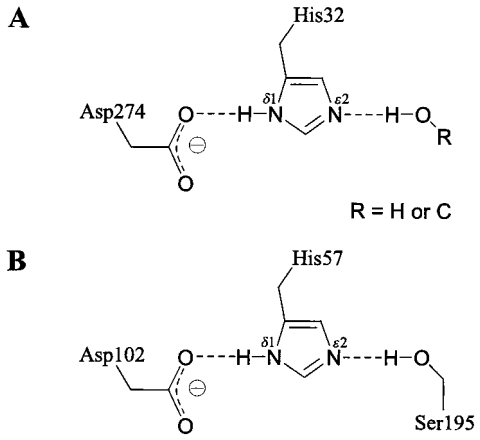

FIGURE 2: Comparison of the Asp-His catalytic diad in PI-PLC (A) and the catalytic triad of serine proteases (B) exemplified by α-chymotrypsin. R represents either a hydrogen atom of water or the C2 carbon atom of *myo*-inositol.

more complex eukaryotic PI-PLCs. For these reasons, the bacterial PI-PLCs have recently been the subject of numerous structural, kinetic, and mechanistic studies as reviewed in (*3*, *4*).

The crystal structures of *B. cereus* and *L. monocytogenes* PI-PLCs have been determined (*5*−*7*). The enzyme consists of a single domain, an irregular $(\beta\alpha)_8$ fold with the active site at the C-termini of the β strands, characteristic of triosephosphate isomerase (TIM) barrel-containing structures. It was postulated from the crystal structure that active site residues Asp274 and His32 form a catalytic diad, which together with the 2-OH of *myo*-inositol of the substrate forms a catalytic triad analogous to the well-known catalytic triad of serine proteases and lipases (Figure 2). This is a novel example of substrate-assisted catalysis (*8*). There is some evidence supporting this hypothesis: Site-directed mutagenesis has established that Asp274 and His32 are required for activity (*5*), and methylation of the 2-OH group of the substrate abolishes activity (*9*).

A key issue is the nature of the hydrogen bonding in the Asp274-His32 catalytic diad. Important information on catalytic diads and triads can be gained from NMR, in cases where low-field (deshielded) proton resonances are resolved (*10*−*12*). Earlier we observed a deshielded line in the ^{1}H NMR spectrum of *B. cereus* PI-PLC during the course of a study of histidine residues (*13*). Here we report a detailed study of the low-field line position and line shape, providing new insights regarding the hydrogen bonding and dynamics of the Asp274-His32 catalytic diad of *B. cereus* PI-PLC.

EXPERIMENTAL PROCEDURES

Materials. Radiolabeled PI (^{3}H-PI) was from NEN (Boston, MA) and bovine liver PI from Avanti Polar Lipids, Inc. (Alabaster, AL). Tris-d_{11} and maleic acid-d_2 were purchased from Cambridge Isotope Laboratories (Andover, MA). NMR tubes were from Wilmad Glass Co., Inc. (Buena, NJ). The concentration of *B. cereus* PI-PLC in solution was determined from the absorbance at 280 nm using a calculated $E^{1\%}$ of 18.4 (molar extinction coefficient of 6.4×10^4 M^{-1} cm^{-1}).

Site-Directed Mutagenesis. The H32A mutant was generated previously (*14*). The D274A mutant PI-PLC was generated using the Chameleon kit (Stratagene, La Jolla, CA), following the procedures recommended by the manufacturer. A single nucleotide substitution was introduced into pHS475, the expression vector for recombinant *B. cereus* PI-PLC. This vector is identical to pIC (*15*) except that 3 kbp of noncoding *B. cereus* sequence have been deleted. The phosphorylated selection primer *Alw*NI → *Nru*I was purchased from Stratagene. The mutagenic primer for D274A, 5′-CATTTATG-TAGGCTTGAATTACCCAGCC-3′ (the replaced base is underlined), was from Biosource International (Camarillo, CA). The mutagenic primer was phosphorylated with T4 polynucleotide kinase (New England Biolabs, Inc., Beverly, MA) and purified using SELECT-D G-25 spin columns (5 Prime → 3 Prime, Inc., Boulder, CO). The region containing the mutation was sequenced using the Sequenase Version 2.0 DNA sequencing kit (Amersham, Cleveland, OH).

Protein Purification, Enzyme Activity Assay, and Buffer System. Recombinant wild-type and mutant *B. cereus* PI-PLCs were purified as described (*16*). The enzyme activity was assayed at pH 7.0 and 37 °C with ^{3}H-PI substrate solubilized in sodium deoxycholate as described previously (*14*). The purified proteins were exchanged into 20 mM Tris-d_{11}-maleate-d_2 buffer for NMR experiments. For the pH-dependence study, the protein samples in 20 mM Tris-d_{11}-maleate-d_2/10% D_2O were adjusted to the desired pH by addition of either 20 mM Tris-d_{11}/10% D_2O or 20 mM maleic acid-d_2/10% D_2O. The pH values were not corrected for the isotope effect. For the pH titration of the low-field peak at 6 °C, the pH meter and electrode were calibrated in a cold room at this temperature, and pH values were measured before and after the acquisition of each spectrum. The concentrations of the maleate buffer components, $[MA^{2-}]$ and $[MAH^-]$, and the Tris buffer components, [Tris] and $[TrisH^+]$, required for the intrinsic chemical exchange rate calculations were determined from the following relationships derived from the acid dissociation equilibria: $[MA^{2-}] = Aw$; $[MAH^-] = A(1 - w)$; $[TrisH^+] = Bz$; $[Tris] = B(1 - z)$; where $w = K_{a2}^{MA}/([H^+] + K_{a2}^{MA})$, $z = [H^+]/([H^+] + K_a^{Tris})$, K_{a2}^{MA} is the second ionization constant of maleic acid, K_a^{Tris} is the dissociation constant of $TrisH^+$, $A = (Tz + [H^+])/(1 + w + z)$, and $B = T - A$. At 6 °C, $pK_{a2}^{MA} = 6.23$ and $pK_a^{Tris} = 8.63$ (Table 1). The maleate is added as maleic acid (MAH_2). The quantity A is the initial concentration of MAH_2. In the pH range examined, the maleic acid dissociates completely, and only MAH^- and MA^{2-} are present in significant concentrations. Tris is added in the unprotonated form, and B is the initial concentration of Tris. The pH is adjusted using aliquots of two equimolar stock solutions so that T, the total concentration of buffer species present, is constant at 2×10^{-2} M.

NMR Spectroscopy. All NMR spectra were acquired on a GE Omega 500 MHz NMR spectrometer using an 8 mm triple-resonance ^{1}H/^{13}C/^{15}N probe with gradient (Nalorac, Martinez, CA). Except where stated otherwise, ^{1}H chemical shifts were referenced to the external standard 2,2-dimethyl-2-silapentane-5-sulfonate (DSS) at 0 ppm. The 1D ^{1}H spectra were acquired using a jump−return pulse sequence (*17*) to maximize the intensity of the resonance of interest. A total of 2500−5000 transients were accumulated for the spectra. The spectral width was 16 129 Hz, and 2048 complex data points were collected with a 200 ms delay between scans.

Table 1: Hydrogen Exchange of the Imidazolium Cation in Aqueous Solution: Second-Order Rate Constants Used for Intrinsic Exchange Rate and Line Shape Calculations

$ImH^+ + X \underset{k_r^X}{\overset{k_f^X}{\rightleftharpoons}} Im + XH^+$ or $ImH^+ + X^- \underset{k_r^X}{\overset{k_f^X}{\rightleftharpoons}} Im + XH$

	Acceptor X[a]	pK_a^{XH}[b]	k_f^X ($M^{-1}s^{-1}$)	k_r^X ($M^{-1}s^{-1}$)
$pK_a^{Im} = 6.95$, 25 °C				
	OH^-[c]	15.74[d]	2.3×10^{10}	45
	H_2O[c]	−1.74[e]	31	1.5×10^{10}
	MA^{2-}[f,g]	6.23[h]	6.5×10^6	3.4×10^7
	Tris[f,g]	8.07[i]	3.0×10^9	2.2×10^8
$pK_a^{Im} = 8.10$, 6 °C				
	OH^-[g,j]	16.43[d]	1.6×10^{10}	75
	H_2O[g,j]	−1.74[e]	2	1.1×10^{10}
	MA^{2-}[g,k]	6.23[l]	5.6×10^5	4.2×10^7
	Tris[g,k]	8.63[m]	8.0×10^8	2.4×10^8

[a] X is the acceptor of the ImH^+ proton in the forward reaction. [b] pK_a of the protonated acceptor X. [c] Rate constants reported by Eigen and Hammes (*22*). Errors range from ±15% to ±35% (*21*). [d] pK_a from (*49*). [e] The pK_a of hydronium ion results from an equilibrium constant $K_{eq} = 1$ and $[H_2O] = 55.5$ M. [f] k_r^X from graph log k vs ΔpK_a (*22*, *43*), and k_f^X is given by $\log k_f^X - \log k_r^X = pK_a^{XH} - pK_a^{Im}$. [g] Errors of up to ±35% are associated with the calculated k_f^X and k_r^X values, reflecting the error of the data from which they were derived. [h] pK_a from (*43*). [i] pK_a from (*50*). [j] Rates calculated from given ΔpK_a at 6 °C and applying $E_a = 3$ kcal mol^{-1} to the fast rate at 25 °C. [k] Rates calculated from given ΔpK_a at 6 °C, the corresponding k_r^X from graph log k vs ΔpK_a at 25 °C (*22*, *43*), and subsequent conversion from 25 to 6 °C using $E_a = 3$ kcal M^{-1} for both rates. [l] The pK_a of MA^{2-} is essentially the same at 25 and 6 °C [ionization enthalpy = −0.83 kcal mol^{-1} (*50*)]. [m] Calculated from pK_a at 25 °C using an enthalpy of ionization of 11.5 kcal mol^{-1} (*50*), and confirmed experimentally.

Data were processed using FELIX software (version 2.30, BioSym Technologies). For all 1D spectra, zero-filling to 8K points and exponential multiplication of 20 Hz were applied. Baselines were corrected with a fifth-order polynomial.

D/H Fractionation Factor Determination. The fractionation factor was determined as described by Loh and Markley (*18*). The samples were prepared as follows: A sample containing 13.5 mg/mL (0.39 mM) wild-type PI-PLC in 20 mM Tris-d_{11}-maleate-d_2, pH 6.6, was divided into six aliquots. Care was taken to ensure that the six aliquots contain equal amounts of protein. A final concentration of 0.5 mM DSS was present in each sample to serve as the internal standard for normalization of the integrals, and 5 μM $MnCl_2$ was added to relax the water resonance during the NMR experiments. After lyophilization overnight, aliquots were dissolved in 1.1 mL of H_2O/D_2O using a different ratio for each aliquot. The dissolved samples were equilibrated at 5 °C for 3 days, and 1D ^{1}H NMR spectra were acquired for each sample at 7 °C. The data points were fitted by nonlinear regression using the program GraFit (Erithacus Software Ltd., Staines, U.K.). One sample was dissolved in 99.9% D_2O as a control for H/D exchange completeness. The low-field resonance of this sample was not observable.

The Position of the Low-Field Line as a Function of pH. In buffer, the His32 $N^{\epsilon 2}$ proton exchange rate with solvent species is fast compared to the differences in chemical shifts involved, so the observed chemical shift, δ_{obs}, for the His32 $N^{\delta 1}$ proton is the weighted average $\delta_{obs} = P_A\delta_A + P_B\delta_B$, where A and B refer to the imidazolium cation (ImH^+) and the neutral imidazole (Im) ring of histidine 32, respectively. δ_A and δ_B are the chemical shifts of protonated and neutral species, and P_A and P_B are the corresponding mole fractions, so that

$$\delta_{obs} = \frac{\delta_A + \delta_B\dfrac{K_a}{[H^+]}}{1 + \dfrac{K_a}{[H^+]}} = \frac{\delta_A + \delta_B 10^{(pH-pK_a)}}{1 + 10^{(pH-pK_a)}} \quad (1)$$

The low-field resonance was titrated over the pH range of 4.1−9.1 at 6 °C, and the shift in line position was fitted to a pK_a using eq 1. The quantities δ_A, δ_B, and pK_a were fitted parameters determined using GraFit. The enzyme concentration in the sample varied between 0.65 and 0.25 mM.

Fast Exchange Rates. The line broadening due to incomplete averaging, ΔW, in the fast exchange regime is given by (*19*, *20*)

$$\Delta W = P_A P_B 4\pi(\Delta\upsilon_{AB})^2\tau \quad (2)$$

where $\Delta\upsilon_{AB}$ is the difference between the two line positions (in frequency units) in the absence of exchange, and τ is the reduced lifetime:

$$\frac{1}{\tau} = \frac{1}{\tau_A} + \frac{1}{\tau_B} \quad (3)$$

and τ_A and τ_B are the mean lifetimes of the protons on the two sites A and B. The fractional populations P_A and P_B were calculated for $pK_a = 8.1$. To obtain the experimental values of ΔW, the total line width at half-height of the low-field line was measured at each pH, and a constant line width, representing the intrinsic line width in the absence of exchange, was subtracted from each value. At 6 °C, the line width was about 140 Hz in the low-pH region (4−5), then increased with rising pH, passing through a maximum at pH 8.1, and then decreased again to about 140 Hz at pH 9. This limiting value of 140 Hz at low and high pH was taken as the intrinsic line width. Likewise, $\Delta\upsilon_{AB}$ was determined from $\Delta\delta$, the difference between the limiting chemical shifts of the low-field line at low and high pH values, obtained by fitting the pH dependence of the low-field peak position. With $\Delta\delta = 2.96$ ppm and an NMR spectrometer frequency of 500 MHz, $\Delta\upsilon_{AB} = 1.48 \times 10^3$ s^{-1} according to $\Delta\upsilon_{AB} = \Delta\delta \times$ NMR frequency $\times 10^{-6}$.

Proton Exchange Rate Kinetics. In aqueous solution with no buffer present, the two reactions responsible for hydrogen exchange of an imidazole group are

$$ImH^+ + H_2O \underset{k_r^{H_2O}}{\overset{k_f^{H_2O}}{\rightleftharpoons}} Im + H_3O^+ \quad (4)$$

and

$$ImH^+ + OH^- \underset{k_r^{OH^-}}{\overset{k_f^{OH^-}}{\rightleftharpoons}} Im + H_2O \quad (5)$$

Thus, the rate of the forward reaction, $rate_f$, and that of the reverse reaction, $rate_r$, are

$$rate_f = \{k_f^{H_2O}[H_2O] + k_f^{OH^-}[OH^-]\}[ImH^+] \quad (6)$$

and

$$rate_r = \{k_r^{H_2O}[H_3O^+] + k_r^{OH^-}[H_2O]\}[Im] \quad (7)$$

The terms in the braces are the pseudo-first-order rate constants, and the terms in brackets are the molar concentrations of ImH^+ and Im. In the presence of the Tris-maleate buffer system, two additional equilibria are introduced:

$$ImH^+ + Tris \underset{k_r^{Tris}}{\overset{k_f^{Tris}}{\rightleftharpoons}} Im + TrisH^+ \quad (8)$$

and

$$ImH^+ + MA^{2-} \underset{k_r^{MA^{2-}}}{\overset{k_f^{MA^{2-}}}{\rightleftharpoons}} Im + MAH^- \quad (9)$$

Thus, the pseudo-first-order rate constant, k_A, for the deprotonation of ImH^+ in the presence of buffer is given by

$$1/\tau_A = k_A = k_f^{H_2O}[H_2O] + k_f^{OH^-}[OH^-] + k_f^{Tris}[Tris] + k_f^{MA^{2-}}[MA^{2-}] \quad (10)$$

And the pseudo-first-order rate constant, k_B, for the protonation of Im in the presence of buffer is

$$1/\tau_B = k_B = k_r^{H_2O}[H_3O^+] + k_f^{OH^-}[H_2O] + k_r^{Tris}[TrisH^+] + k_r^{MA^{2-}}[MAH^-] \quad (11)$$

Since the equations are pseudo-first-order, the lifetimes τ are inversely proportional to the pseudo-first-order rate constants, and are independent of the concentration of ImH^+ and Im. The intrinsic rate constant of a free imidazole, $k_{ex}^{intrinsic}$, was calculated by summing k_A and k_B from eqs 10 and 11.

Protection Factors. The protection factor P is defined by $P = k_{ex}^{intrinsic}/k_{ex}^{obsd}$ where the pseudo-first-order rate constant $k_{ex}^{obsd} = 1/\tau$ is obtained from the experimental NMR line widths and eqs 2 and 3. The intrinsic rate constant for a free imidazole, $k_{ex}^{intrinsic}$, is the product of the concentration of catalytic species times the second-order rate constants for hydrogen exchange reactions of imidazole. The second-order rate constants were estimated from relaxation data and equilibria measurements for an imidazole with $pK_a = 6.95$ at 25 °C, as listed in the top half of Table 1 (*21*, *22*). The values for His32 with $pK_a = 7.6$ at 25 °C, corresponding to 8.10 at 6 °C, were estimated from these kinetic data and thermodynamic data (lower half of Table 1).

NMR Line Shape Calculations. Line shape simulations were based on the classical Bloch equations, modified for chemical exchange between two sites (*20*, *23*). Calculations were performed in MathCad (MathSoft, Inc., Cambridge, MA) using the formalism of Nakagawa (*24*).

RESULTS

Assignment of the Deshielded Proton Resonance of PI-PLC. A single broad resonance was observed at 16.4 ppm at pH 6.3 in the ^1H NMR spectrum at 500 MHz for a solution of the wild-type *B. cereus* PI-PLC in buffered H_2O. From the crystal structure, His32 is within hydrogen bonding distance of Asp274. For this reason, alanine mutants of His32 and Asp274 were prepared and examined by NMR. The low-field peak was not present in the spectrum of either the H32A or the D274A mutant. The enzyme activity was measured for these mutants and found to be virtually abolished, yielding only about (3×10^{-6})-fold of the wild-type activity [1.0×10^{-4}% and 3.4×10^{-4}% of wild type for H32A (*14*) and D274A, respectively]. For comparison, the activity of the D274N mutant is 4.2% of wild type. This mutations has a much less severe effect on catalysis, probably because the presence of an Asn side chain in residue 274 still allows the formation of a hydrogen bond with His32 (*25*).

D/H Fractionation Factor. The D/H fractionation factor, ϕ, for the $N^{\delta 1}$ site of His32 is the equilibrium constant for the equilibrium isotope exchange reaction:

$$N^{\delta 1}-H + S-D \rightleftharpoons N^{\delta 1}-D + S-H$$

where S is the solvent (*11*, *18*). The preliminary value obtained utilizing one set of five data points (i.e., enzyme in 5%, 15%, 30%, 50%, and 75% D_2O) at pH 6.6 and 7 °C was $\phi = 0.79$, with a probable uncertainty of ±0.11. This must be regarded as a preliminary value since the duplicate determination was not performed under exactly the same conditions.

Slow Exchange of the His32 $N^{\delta 1}$ Proton with Solvent. When D_2O was added, the low-field NMR peak disappeared in a time shorter than the 15 min required for inserting the sample in the NMR spectrometer and collecting the spectrum. When the H_2O line was saturated, the low-field resonance was also saturated. Thus, during the characteristic relaxation time T_1 of water, solvent protons experience both the environment of His32 and that of the solvent. Since T_1 of the water protons is about 1 s, this indicates that the exchange rate is greater than 1 s^{-1}. From the intrinsic width of the low-field line, i.e., the minimum line width, the upper limit of the exchange rate is about 3×10^2 s^{-1} (Table 2). The line width at pH 6.3 increased with increasing temperature over the range 6−25 °C. Assuming this increase is entirely due to the exchange process, a plot of the log of the change in line width vs $1/T$ gives an estimate of the exchange rate of $\sim 1 \times 10^2$ s^{-1} at 6 °C and an activation energy of 13 kcal/mol.

Rapid Exchange of the His32 $N^{\epsilon 2}$ Proton with Solvent. The His32 $H^{\epsilon 2}$ resonance was not observed, indicating that the rate of exchange was rapid on the NMR time scale. However, the low-field peak $H^{\delta 1}$ line shifted from 16.3 ppm at pH 4 to 13.8 ppm at pH 9 (Figure 3A). The pK_a derived from the titration points is 8.0 at 6 °C (Figure 3B). The pK_a of His32 is 7.6 at 25 °C (*14*). It is known that the dissociation of the imidazole cation into a neutral imidazole and a proton is accompanied by a large positive standard enthalpy change, $\Delta H°$. Thus, the pK_a increases as the temperature is decreased. For a free histidine, $\Delta H° = 6.8$ kcal/mol at 25 °C (*26*, *27*). From the van't Hoff equation, a $pK_a = 7.6$ at 25 °C for an imidazole with this enthalpy change corresponds to $pK_a = 8.06$ at 6 °C, in agreement with $pK_a = 8.0$ derived from the titration and $pK_a = 8.1$ used in line shape simulations. This is consistent with the conclusion that the origin of the shift of the low-field His32 $H^{\delta 1}$ NMR line is the state of protonation of His32. The peak intensity remains approximately constant, while the line shape changes with pH. The line shape change is caused by a modulation of the

Table 2: Chemical Shift and Exchange Rates of the His $N^{\delta 1}$ Proton in PI-PLC and Comparison with a Serine Protease

system	pH	δ (ppm)	assignment and interaction	k_{ex}^{obsd} (s^{-1})	$k_{ex}^{intrinsic}$ (s^{-1})	protection factor
PI-PLC[a]	9	13.8	$Asp^{(-)}\cdots H^{\delta 1}-His^{(0)}$	$\leq 3 \times 10^2$	1.1×10^7	$\geq 4 \times 10^4$
	6	16.4	$Asp^{(-)}\cdots H^{\delta 1}-His^{(+)}$	$\leq 3 \times 10^2$	3.0×10^6	$\geq 1 \times 10^4$
chymotrypsinogen[b]	9	15.2	$Asp^{(-)}\cdots H^{\delta 1}-His^{(0)}$	3.5×10^3	1.1×10^4	3.0
	3.5	18.1	$Asp^{(-)}\cdots H^{\delta 1}-His^{(+)}$	9.5×10^2	8.7×10^3	9.2
	1	18.0	$Asp^{(0)}\cdots H^{\delta 1}-His^{(+)}$	3.9×10^3	8.7×10^3	2.2

[a] This study. Errors in δ are ± 0.05 ppm. The Asp274 pK_a is assumed to be ≤ 5. [b] From (*12*).

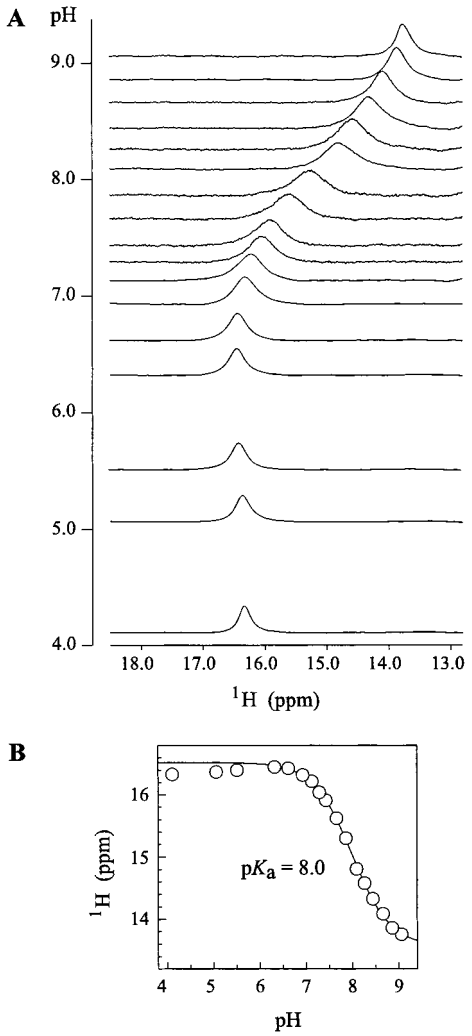

FIGURE 3: pH dependence of the low-field resonance in the 500 MHz ^{1}H NMR spectrum of *B. cereus* PI-PLC. (A) Individual spectra acquired at 6 °C and pH values ranging from 4.1 to 9.0 in 20 mM Tris-maleic acid buffer/10% D_2O. The baseline of each spectrum is aligned with the pH value at which it was obtained. (B) Plot of the peak positions of the spectra in (A) as a function of pH. The curve was obtained by fitting the data to eq 1 with pK_a = 8.0.

magnetic environment of His32 $H^{\delta 1}$ due to rapid chemical exchange of His32 $H^{\epsilon 2}$ with solvent molecules. The exchange rate was calculated from the line broadening (ΔW) as a function of pH using eq 2, and selected values are given in Table 3.

Protection Factors for His32 Protons. The calculated pseudo-first-order proton exchange rate constant for a free imidazole in 20 mM Tris-maleate buffer at 6 °C and the corresponding protection factor for His32 $H^{\delta 1}$ are given in Table 2. At pH 6, the dominant term from eqs 10 and 11 was k_r^{Tris}[$TrisH^+$], and at pH 9, the dominant term was k_f^{Tris}[Tris]. The contributions of the maleate were smaller than Tris throughout the pH range of interest (pH 4−9). In the absence of buffer, the rate constants are much smaller. For example, $k_{ex}^{intrinsic}$ for an imidazole with pK_a = 8.1 in an aqueous solution without buffer was calculated to be 3.7×10^4 s^{-1} at pH 9 and 1.5×10^4 s^{-1} at pH 6. These values are 2 orders of magnitude smaller than the corresponding rate constant in the presence of buffer (Table 2), and are similar to the intrinsic rate constants calculated for chymotrypsinogen by Markley and Westler (*12*), which are listed for comparison in Table 2. The intrinsic rate constants for $H^{\epsilon 2}$ given in Table 3 were calculated by the same procedure for a pK_a of 7.4, reflecting the fact that the pK_a of $H^{\epsilon 2}$ is known to be about 0.7 pK_a unit lower than that of the imidazole $H^{\delta 1}$ (*12*, *28*).

Line Shape Simulations. Line shapes as a function of pH were calculated using general solutions to the classical Bloch equations modified for exchange between two sites, valid for slow and intermediate exchange as well as fast exchange. The basis of the calculation is that the His32 $H^{\delta 1}$ NMR line width is modulated by pH-dependent exchange of the His32 $N^{\epsilon 2}$ proton with solvent. The only parameter is a scaling factor applied to all terms (i.e., an average protection factor). A representative set of line shapes as a function of pH is given in Figure 4. In the presence of buffer, the average protection factor for His32 $H^{\epsilon 2}$ which best fit the set of line shapes over the entire pH range of 4−9 was 120. The calculated exchange rates predict that the low-field line becomes much broader in the absence of buffer, and too broad to be detectable at the intermediate pH values. This is in agreement with experiment. For example, no low-field peak in the ^{1}H NMR spectrum was detected for a 0.27 mM PI-PLC sample at pH 8.5 and 6 °C without buffer.

DISCUSSION

Assignment, Line Position, and Bond Distances. This study has used a combination of site-directed mutagenesis, ^{1}H chemical shifts, and an exchange rate analysis to characterize the Asp-His catalytic diad in *B. cereus* PI-PLC. The X-ray crystal structure of *B. cereus* PI-PLC shows that the $N^{\delta 1}$ atom of His32 is within hydrogen bonding distance (2.6 Å) from the $O^{\delta 1}$ atom of Asp274 (*5*). Mutation of either His32 or Asp274 to alanine essentially abolished enzymatic activity, and the low-field NMR peak is missing in these mutants. We therefore assigned the low-field peak to the histidine $H^{\delta 1}$ forming the Asp274−His32 hydrogen bond in *B. cereus* PI-PLC. The crystal structures of several His32 and Asp274 mutants of *B. cereus* PI-PLC, including H32A, H32L, D274N, and D274S, have been examined, and there are no significant tertiary structural changes compared to wild type (*25*).

A deshielded histidine imidazole proton resonance is indicative of a significant hydrogen bond, the nature of which

Table 3: NMR-Derived Properties of the His $N^{\epsilon 2}$ Proton in PI-PLC and Comparison with a Serine Protease

system	pH	δ (ppm)	assignment and interaction	k_{ex}^{obsd} (s^{-1})	$k_{ex}^{intrinsic}$ (s^{-1})	protection factor
PI-PLC[a]	9	not seen	$His^{(+)}-H^{\epsilon 2}\cdots X$	1.7×10^5	5.1×10^7	3.0×10^2
	6	not seen	$His^{(+)}-H^{\epsilon 2}\cdots X$	1.7×10^4	3.1×10^6	1.8×10^2
chymotrypsinogen[b]	3.5	13.2	$His^{(+)}-H^{\epsilon 2}\cdots Ser^{(0)}$	3.8×10^2	1.7×10^3	4.5
	1	13.4	$His^{(+)}-H^{\epsilon 2}\cdots Ser^{(0)}$	1.2×10^3	1.7×10^3	1.4

[a] This study. X is the proton acceptor (solvent or buffer component). Errors in the observed exchange rates k_{ex}^{obsd} are ± 0.5 s^{-1}. [b] From (*12*).

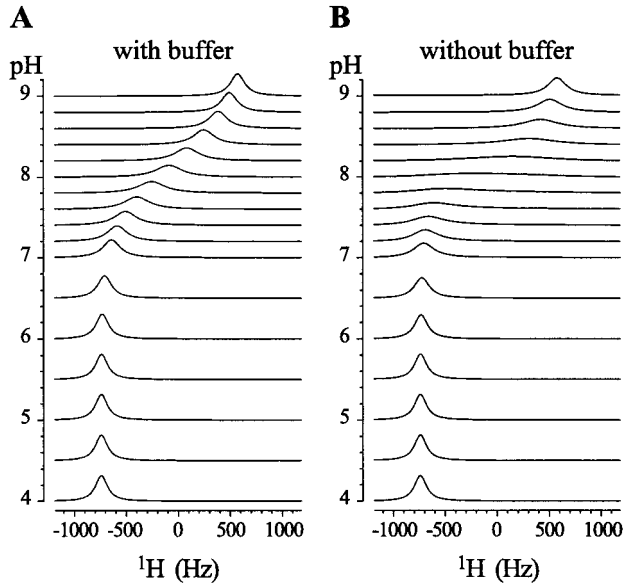

FIGURE 4: Calculated line shapes for the low-field region in the presence (A) and absence (B) of 20 mM Tris-maleic acid buffer. The spectra were obtained utilizing the general Bloch equations modified to include exchange between two sites. Input parameters: pK_a values and second-order rate constants for hydrogen exchange with imidazole at 6 °C (bottom half of Table 1), intrinsic line width in the absence of exchange = 140 Hz, NMR spectrometer frequency = 500 MHz, and a protection factor of 120. In the absence of buffer, the exchange rates are reduced, and the simulations predict that the line width is broadened beyond detection at intermediate pH values, in agreement with experiment.

is a topic of broad interest (*29*−*32*). The earliest observations of deshielded proton NMR lines were on chymotrypsin and chymotrypsinogen (*19*, *33*). These and other serine proteases are being investigated in a number of laboratories (*12*, *30*, *34*, *35*). A growing number of other proteins including cholinesterases (*36*, *37*) and triosephosphate isomerase (*11*) also exhibit deshielded proton NMR lines that have been classified as short, strong hydrogen bonds (SSHB) by NMR criteria. NMR provides hydrogen bond length through correlations with high-resolution crystal structure data on model systems, and exchange rate information. NMR does not provide a thermodynamic value of the bond strength, and indeed that is difficult to obtain by any method on proteins because of the many hydrogen bonds involved and the aqueous environment. NMR data on bond lengths are important because most protein X-ray crystallographic studies do not observe the hydrogens directly, and the resolution is insufficient to distinguish between small changes in bond distances, which can correspond to large differences in bond strengths (*38*). Viragh et al. (*36*) have reported a correlation of the imidazolium−carboxylate hydrogen bond distances based on the data reported by Wei and McDermott (*39*) on high-resolution, small-molecule X-ray diffraction measurements and proton chemical shifts from solid-state NMR studies of amino acids. The empirical formula is $D = 1.99 + 0.198 \ln(\delta) + (10.14/\delta)^5$ where D is the distance between the two electronegative atoms in angstroms and δ is the chemical shift in ppm. By this formula, the chemical shift of 16.4 ppm for the low-field line measured at pH 6 (Table 2) corresponds to an Asp−His hydrogen bond distance of 2.63 ± 0.04 Å [essentially the same value can be interpolated from Figure 1B of reference (*39*)]. This may be compared to the X-ray crystallographic value of 2.6 ± 0.3 Å (*5*). Furthermore, the D/H fractionation factor (ϕ) is less than 1. A value of 0.79 ± 0.11 at pH 6.7 corresponds to an Asp−His hydrogen bond distance of 2.63 Å, using the methods described by Bao et al. (*35*), and the assumptions employed by Harris and Mildvan (*40*). Thus, both NMR measurements of the hydrogen bond distance are in agreement with the X-ray crystallography data. The NMR chemical shift data provide the most accurate determination of the hydrogen bond length in this case. The downfield shift from pH 9 to pH 6 indicates a shortening of the hydrogen bond as His32 is protonated, a result of the reduction in the mismatch of the pK_a values of Asp274 and His32. This decrease in chemical shift parallels that observed for chymotrypsinogen (Table 2) and other serine proteases. Like PI-PLC, the fractionation factors of the corresponding protonated His $N^{\delta 1}$ in serine proteases are less than unity; e.g., $\phi = 0.40$ for chymotrypsinogen at pH 3.5 (*41*) and $\phi = 0.64$ for chymotrypsin at pH 3 (*35*).

Recently, a high-resolution X-ray and neutron diffraction study of a model compound which contains an Asp-His diad was reported (*42*). The compound, a cocrystal of betaine, imidazole, and picric acid, contains a two-center hydrogen bond between a positively charged imidazole and a negatively charged carboxyl group with an overall N···O distance of 2.685 Å. The hydrogen atoms are resolved, and the positions indicate two separate harmonic potential wells. The hydrogen is localized at the nitrogen atom (i.e., N−H···O). Estimates based on charge densities indicate the H···O bond energy exceeds that of a normal hydrogen bond (2−10 kcal mol^{-1}). This model diad contains a short, strong hydrogen bond that is not a low barrier hydrogen bond (LBHB) or a single well potential hydrogen bond. The distance between the N and O is shortened and the N−H bond is lengthened compared to an N−H group in the absence of hydrogen bonding. This and other model systems (*39*), and the present NMR results, support the conclusion that the Asp-His catalytic diad of PI-PLC forms a short, strong hydrogen bond (SSHB) but not a LBHB, under the conditions examined.

Proton Exchange Rates. The NMR data provide detailed information about the exchange rates of the Asp-His catalytic diad. The data are summarized in Tables 2 and 3, and in Figure 5. The His32 $N^{\delta 1}$ proton hydrogen-bonded to Asp274

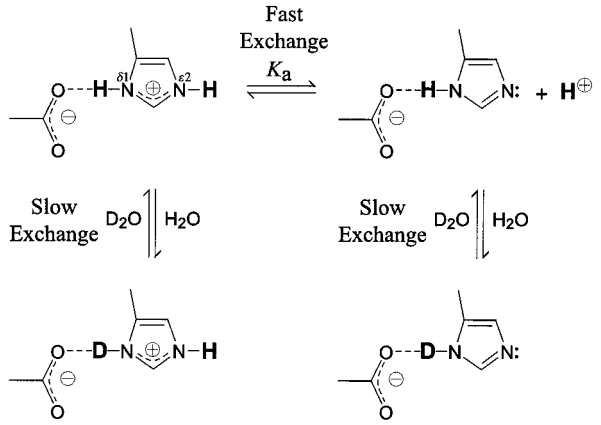

FIGURE 5: Summary of the hydrogen bonding dynamics of the Asp-His catalytic diad at the active site of *B. cereus* PI-PLC. The low-field NMR line provides a direct observation of the $N^{\delta 1}$ proton of the hydrogen bond formed between Asp274 and His32. This hydrogen is solvent-accessible, but the rate of exchange with solvent protons is slow on the NMR time scale. The $N^{\epsilon 2}$-H of His32 undergoes a rapid deprotonation−protonation reaction.

exchanges slowly with solvent on the NMR time scale, whereas the $N^{\epsilon 2}$ proton exchanges rapidly with solvent. Both observations are consistent with the crystal structure, which shows the catalytic diad to be in a protected but accessible position in the active site pocket. Surprisingly, the exchange rate of the $N^{\delta 1}$ proton is slower than is reported for the corresponding proton of catalytic triads of serine proteases (Table 2). The protection factor for the $N^{\delta 1}$ proton in PI-PLC is much greater than that reported previously for the serine proteases. One contributing factor is the lower exchange rate of the protons of the PI-PLC catalytic diad. Another factor is the choice of buffer system. The present study was carried out in Tris-maleate buffer to facilitate the control of pH and because the enzyme was known to be stable and active in this environment. The Tris and maleate buffer components greatly enhance $k_{ex}^{intrinsic}$, the intrinsic exchange rate of a free imidazole, because ΔpK_a values, the difference between the pK_a values of the acceptor and donor of the hydrogen, are relatively small. Proton transfer occurs by the formation of labile hydrogen bridges between donor and acceptor (*43*). The generally accepted kinetic model for hydrogen exchange is based on the assumption that a labile hydrogen atom in a protein can exchange only after the breakage of any hydrogen bonds it forms with other residues in the protein, so that it is fully exposed to solvent (*44*, *45*). There are two limiting cases; in one (designated EX_1), the exchange rate is essentially the rate of breaking the hydrogen bond and exposing the proton to solvent, and in the other (EX_2), the catalysis step is limiting. The pH dependence of the rate constant and the observation that the buffer has a large effect on the rate constant suggest that the exchange kinetics are at or very near the EX_2 limiting case for the proton shared in the Asp274-His32 diad.

Catalytic Mechanism and Substrate-Assisted Catalysis. The NMR results support the catalytic mechanism shown in Figure 6, which summarizes the structural and mechanistic studies of many laboratories. *B. cereus* PI-PLC has features in common with both ribonuclease A and the serine proteases. Like ribonuclease A, it is a concerted general acid−base-catalyzed reaction involving two histidines. His32 is the general base, assisted by Asp274, and His82 is the acid,

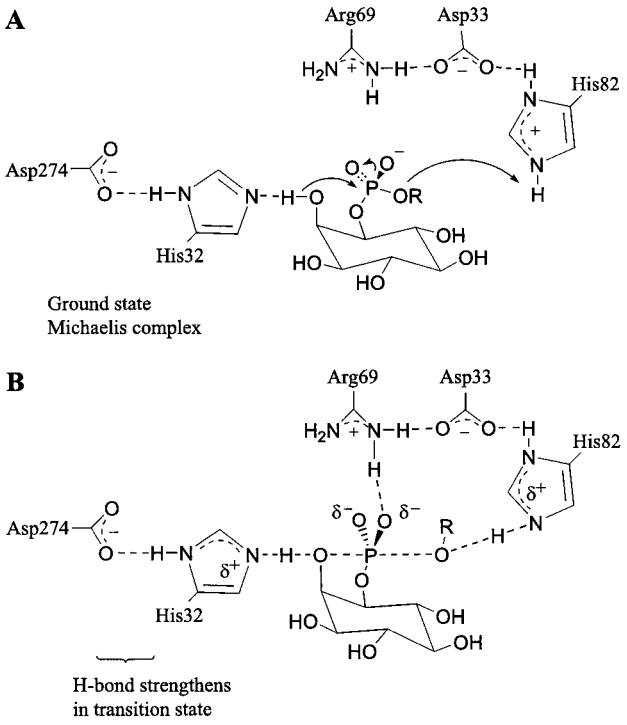

FIGURE 6: The catalytic mechanism of *B. cereus* PI-PLC shares features with both ribonuclease A and the serine proteases. (A) In the ground-state Michaelis complex, the *myo*-inositol moiety of the substrate assists by providing the nucleophile, 2-OH. Asp274, His32, and the 2-OH of *myo*-inositol form a triad similar to the catalytic triad of serine proteases. His32, together with Asp274, activates the 2-OH, which then carries out a nucleophilic attack on phosphorus. (B) Proposed pentacovalent transition state showing the positive charge buildup on His32. The other histidine shown, His 82, acts as the general acid, assisted by Asp33, donating a proton to the leaving group, diacylglycerol (O−R). Arg69 stabilizes the negatively charged phosphate and Asp33. All of these residues probably act in a concerted fashion.

assisted by Asp33. The positively charged Arg69 serves to stabilize the negatively charged phosphate group. The three groups Arg69, Asp33, and His82 are hydrogen-bonded in the crystal structure (*5*), and recently it has been postulated that they act as a second catalytic triad (*46*). Although this is plausible, the hydrogen bonding distance for Asp33−His82 (≥3.2 Å) is much greater than the hydrogen bonding distance for Asp274−His32 (2.6 Å), and we did not observe any deshielded lines arising from His82. Only His32 produces a deshielded line in the ^1H NMR spectrum. The fact that the peak can be observed over a wide temperature range (6−25 °C), and without the necessity of having an inhibitor complexed at the active site, indicates that this hydrogen bond is particularly robust. In the ground-state Michaelis complex, His32 is hydrogen-bonded to the 2-OH of the *myo*-inositol moiety of the substrate. This interaction increases the nucleophilicity of the oxygen atom. As the 2-OH oxygen carries out a nucleophilic attack on phosphorus, the protonated form of His82 begins to donate its hydrogen to the scissile ester bond, producing a good leaving group, diacylglycerol (ROH). In the pentavalent transition state, the attacking 2-OH is at one apex and the leaving group ROH is at the other. After dissociation of the products, the active site is restored to its initial state either by reprotonation of His82 by water or by binding and hydrolysis of cIP to I(1)P.

PI-PLC is an example of substrate-assisted catalysis. Substrate-assisted catalysis occurs when a functional group

of the substrate accelerates the rate of reaction catalyzed by the enzyme. In this case, the substrate provides the nucleophile, 2-OH, which accelerates the reaction, forming the cyclic product. The free 2-OH group is regenerated in a second hydrolysis step. Ribonuclease A and ribozymes can be viewed as other examples, since the 2′-OH of ribose acts in a similar way, providing the nucleophile necessary for attack on phosphorus. There are an increasing number of enzyme mechanisms utilizing substrate-assisted catalysis (*8*). Mutating the catalytic histidine of subtilisin to alanine, for example, essentially abolishes the activity of serine protease. The activity can be partially rescued by incorporating a histidine in the polypeptide substrate. When the substrate is bound at the active site, it is possible to virtually superimpose its imidazole group with that of the corresponding catalytic histidine in the triad (*8*, *47*). Similarly, the Asp-His-Ser catalytic triads of α-chymotrypsin, subtilisin, and lipase superimpose on the substrate-assisted catalytic triad Asp-His-inositol of PI-PLC (*25*). The NMR behavior reported here for the PI-PLC Asp274-His32 diad is remarkably similar to that reported previously for the catalytic triad of serine proteases (*12*, *48*) and a growing list of other enzymes (*36*, *40*), strongly suggesting that the hydrogen bonding of the histidine in these catalytic triads are closely related.

ACKNOWLEDGMENT

We thank Drs. Christopher J. Halkides, Bo B. Iversen, Albert S. Mildvan, and Larry H. Weaver for useful discussions and Carey R. Martens for help in purifying the D274A mutant.

REFERENCES

1. Berridge, M. J. (1993) *Nature 361*, 315−325.
2. Rhee, S. G., Poulin, B., Lee, S. B., and Sekiya, F. (2000) *Front. Mol. Biol. 27*, 1−31.
3. Griffith, O. H., and Ryan, M. (1999) *Biochim. Biophys. Acta 1441*, 237−254.
4. Bruzik, K. S., and Tsai, M. D. (1994) *Bioorg. Med. Chem. 2*, 49−72.
5. Heinz, D. W., Ryan, M., Bullock, T. L., and Griffith, O. H. (1995) *EMBO J. 14*, 3855−3863.
6. Moser, J., Gerstel, B., Meyer, J. E., Chakraborty, T., Wehland, J., and Heinz, D. W. (1997) *J. Mol. Biol. 273*, 269−282.
7. Heinz, D. W., Wehland, J., and Griffith, O. H. (1999) *ACS Symp. Ser. 718*, 80−90.
8. Dall'Acqua, W., and Carter, P. (2000) *Protein Sci. 9*, 1−9.
9. Lewis, K. A., Garigapati, V. R., Zhou, C., and Roberts, M. F. (1993) *Biochemistry 32*, 8836−8841.
10. Schultz, L. W., Quirk, D. J., and Raines, R. T. (1998) *Biochemistry 37*, 8886−8898.
11. Harris, T. K., Abeygunawardana, C., and Mildvan, A. S. (1997) *Biochemistry 36*, 14661−14675.
12. Markley, J. L., and Westler, W. M. (1996) *Biochemistry 35*, 11092−11097.
13. Liu, T., Ryan, M., Dahlquist, F. W., and Griffith, O. H. (1999) *ACS Symp. Ser. 718*, 91−108.
14. Liu, T., Ryan, M., Dahlquist, F. W., and Griffith, O. H. (1997) *Protein Sci. 6*, 1937−1944.
15. Koke, J. A., Yang, M., Henner, D. J., Volwerk, J. J., and Griffith, O. H. (1991) *Protein Expression Purif. 2*, 51−58.
16. Ryan, M., Smith, M. P., Vinod, T. K., Lau, W. L., Keana, J. F. W., and Griffith, O. H. (1996) *J. Med. Chem. 39*, 4366−4376.
17. Plateau, P., and Guéron, M. (1982) *J. Am. Chem. Soc. 104*, 7310−7311.
18. Loh, S. N., and Markley, J. L. (1993) in *Techniques in Protein Chemistry IV* (Angeletti, R., Ed.) pp 517−524, Academic Press, San Diego.
19. Robillard, G., and Shulman, R. G. (1974) *J. Mol. Biol. 86*, 519−540.
20. Carrington, A., and McLachlan, A. D. (1967) *Introduction to Magnetic Resonance*, Harper & Row, New York.
21. Eigen, M., Hammes, G. G., and Kustin, K. (1960) *J. Am. Chem. Soc. 82*, 3482−3483.
22. Eigen, M., and Hammes, G. G. (1963) *Adv. Enzymol. Relat. Areas Mol. Biol. 25*, 1−38.
23. Sandström, J. (1982) *Dynamic NMR Spectroscopy*, Academic Press, London.
24. Nakagawa, T. (1966) *Bull. Chem. Soc. Jpn. 39*, 1006−1008.
25. Gässler, C. S., Ryan, M., Liu, T., Griffith, O. H., and Heinz, D. W. (1997) *Biochemistry 36*, 12802−12813.
26. Boschcov, P., Seidel, W., Muradian, J., Tominaga, M., Paiva, A. C. M., and Juliano, L. (1983) *Bioorg. Chem. 12*, 34−44.
27. Bhattacharya, S., and Lecomte, J. T. (1997) *Biophys. J. 73*, 3241−3256.
28. Boschcov, P., Seidel, W., Muradian, J., Tominaga, M., Paiva, A. C. M., and Juliano, L. (1983) *Bioorg. Chem. 12*, 34−44.
29. Mildvan, A. S., Harris, T. K., and Abeygunawardana, C. (1999) *Methods Enzymol. 308*, 219−245.
30. Ash, E. L., Sudmeier, J. L., De Fabo, E. C., and Bachovchin, W. W. (1997) *Science 278*, 1128−1132.
31. Cleland, W. W., and Kreevoy, M. M. (1994) *Science 264*, 1887−1890.
32. Frey, P. A., Whitt, S. A., and Tobin, J. B. (1994) *Science 264*, 1927−1930.
33. Robillard, G., and Shulman, R. G. (1972) *J. Mol. Biol. 71*, 507−511.
34. Halkides, C. J., Wu, Y. Q., and Murray, C. J. (1996) *Biochemistry 35*, 15941−15948.
35. Bao, D., Huskey, W. P., Kettner, C. A., and Jordan, F. (1999) *J. Am. Chem. Soc. 121*, 4684−4689.
36. Viragh, C., Harris, T. K., Reddy, P. M., Massiah, M. A., Mildvan, A. S., and Kovach, I. M. (2000) *Biochemistry 39*, 16200−16205.
37. Massiah, M. A., Viragh, C., Reddy, P. M., Kovach, I. M., Johnson, J., Rosenberry, T. L., and Mildvan, A. S. (2001) *Biochemistry* (in press).
38. Harris, T. K., Zhao, Q., and Mildvan, A. S. (2000) *J. Mol. Struct. 552*, 97−109.
39. Wei, Y., and McDermott, A. E. (1999) *ACS Symp. Ser. 732*, 177−193.
40. Harris, T. K., and Mildvan, A. S. (1999) *Proteins: Struct., Funct., Genet. 35*, 275−282.
41. Markley, J. L. (1975) *Acc. Chem. Res. 8*, 70−80.
42. Overgaard, J., Schiøtt, B., Larsen, F. K., Schultz, A. J., MacDonald, J. C., and Iversen, B. B. (1999) *Angew. Chem., Int. Ed. Engl. 38*, 1239−1242.
43. Eigen, M. (1964) *Angew. Chem., Int. Ed. Engl. 3*, 1−19.
44. Hvidt, A., and Nielsen, O. S. (1966) *Adv. Protein Chem. 21*, 287−386.
45. Englander, S. W., and Kallenbach, N. R. (1984) *Q. Rev. Biophys. 16*, 521−655.
46. Kubiak, R. J., Hondal, R. J., Yue, X., Tsai, M.-D., and Bruzik, K. S. (1999) *J. Am. Chem. Soc. 121*, 488−489.
47. Wells, J. A., Cunningham, B. C., Graycar, T. P., Estell, D. A., and Carter, P. (1987) *Cold Spring Harbor Symp. Quant. Biol. 52*, 647−652.
48. Lin, J., Westler, W. M., Cleland, W. W., Markley, J. L., and Frey, P. A. (1998) *Proc. Natl. Acad. Sci. U.S.A. 95*, 14664−14668.
49. Covington, A. K., Robinson, R. A., and Bates, R. G. (1966) *J. Phys. Chem. 70*, 3820−3824.
50. Fasman, G. D. (1976) *Handbook of Biochemistry and Molecular Biology, Physical and Chemical Data*, 3rd ed., Vol. 1, CRC Press, Cleveland, OH.

BI010958M